Reflection of a Coaxial Line Radiating Into a Parallel Plate

Jung H. Lee, Hyo J. Eom, and Kyung H. Jun

Abstract—**Reflection of a coaxial line radiating into a parallel plate is solved analytically. The Hankel transform and the mode-matching technique are used to represent the reflection coefficient in rapidly converging series. The numerical computations are performed to illustrate the reflection behavior in terms of coaxial geometries and frequency. The presented series solution is an analytic, closed-form that is simple yet efficient for numerical computation.**

I. Introduction

RADIATION from a flanged coaxial line into a half-space has been extensively studied in [1]–[3] for material permittivity characterization. Radiation from a coaxial line into a parallel-plate was also studied in [4] for antenna application. Note that in [4] the current distribution at the coaxial line aperture is arbitrarily assumed to determine the radiation. It is thus of interest to rigorously determine the aperture current and the reflection coefficient of the coaxial line radiating into a parallel-plate. The purpose of the present paper is to represent the reflection coefficient in rapidly converging series by using the Hankel transform and the mode-matching technique. Our solution is also general in that it reduces to a case of radiation from the flanged coaxial line into a half space, as considered in [1]–[3]. In the next section, we present an analytic solution in simple series form and discuss its numerical behavior. A brief summary is given in Section III.

II. Radiation Analysis

Consider a coaxial line radiating into a conducting parallel plate shown in Fig. 1. Assume an incident TEM mode excites the coaxial line, thereby producing the reflected TEM and all higher TM_{0n} mode inside the coaxial line. In region (I) ($a < r < b$, $z < 0$), the incident and reflected H-fields are

$$H_\phi^i(r, z) = \frac{M_0 e^{i\beta_1 z}}{r} \tag{2.1}$$

$$H_\phi^r(r, z) = c_0 M_0 e^{-i\beta_1 z}/r + \sum_{n=1}^{\infty} c_n M_n R_n(r) e^{-ik_{zn} z} \tag{2.2}$$

where $\beta_1 = \omega\sqrt{\mu\epsilon_1}$, $k_{zn} = \beta_1\sqrt{1-(k_n/\beta_1)^2}$, $R_n(r) = J_1(k_n r)N_0(k_n b) - N_1(k_n r)J_0(k_n b)$, $M_0 = 1/\sqrt{\ln(b/a)}$, and $M_n = \pi k_n/\sqrt{2 - [2J_0^2(k_n b)]/[J_0^2(k_n a)]}$. $J_n(\cdot)$ and $N_n(\cdot)$ are the nth order Bessel and Neumann functions, and k_n is determined by $J_0(k_n a)N_0(k_n b) - N_0(k_n a)J_0(k_n b) = 0$.

Manuscript received September 26, 1995.
The authors are with Department of Electrical Engineering, Korea Advanced Institute of Science and Technology, Taejon, Korea.
Publisher Item Identifier S 1051-8207(96)02063-6.

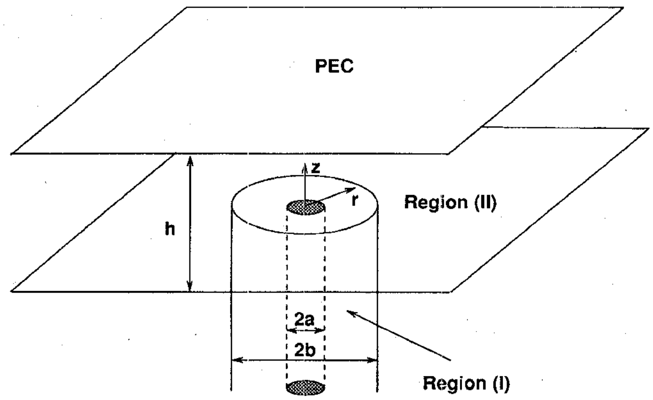

Fig. 1. Problem geometry.

In Region (II) ($z > 0$), the transmitted H-field is

$$H_\phi^t(r, z) = \int_0^\infty \tilde{H}(\zeta)\left[e^{i\kappa z} + e^{2i\kappa h}e^{-i\kappa z}\right] \cdot J_1(\zeta r)\zeta\, d\zeta \tag{2.3}$$

where $\kappa = \sqrt{\beta_2{}^2 - \zeta^2}$, $\beta_2 = \omega\sqrt{\mu\epsilon_2} = 2\pi/\lambda$: wave number.

The tangential E-field continuity at $z = 0$ yields

$$E_r^t(r, 0) = \begin{cases} E_r^i(r, 0) + E_r^r(r, 0), & a < r < b \\ 0, & \text{otherwise.} \end{cases} \tag{2.4}$$

Taking the Hankel transform of (2.4) and solving for $\tilde{H}(\zeta)$

$$\tilde{H}(\zeta) = \frac{\epsilon_2}{\epsilon_1}\frac{1}{\kappa(1 - e^{2i\kappa h})} \cdot \left[(1 - c_0)\beta_1 f_0(\zeta) - \sum_{n=1}^{\infty} c_n k_{zn} f_n(\zeta)\right] \tag{2.5}$$

where

$$f_0(\zeta) = -\frac{M_0[J_0(b\zeta) - J_0(a\zeta)]}{\zeta} \tag{2.6}$$

$$f_n(\zeta) = \frac{2M_n\zeta[J_0(\zeta b)J_0(k_n a) - J_0(\zeta a)J_0(k_n b)]}{\pi k_n J_0(k_n a)(k_n{}^2 - \zeta^2)}. \tag{2.7}$$

The tangential H-field continuity at $z = 0$ gives

$$H_\phi^t(r, 0) = H_\phi^i(r, 0) + H_\phi^r(r, 0), \quad a < r < b. \tag{2.8}$$

Substituting (2.1), (2.2), and (2.3) into (2.8), multiplying (2.8) by $rM_pR_p(r)\,dr$, and integrating from b to a, we then obtain, after algebraic manipulation

$$C=(U-A)^{-1}\Gamma \tag{2.9}$$

where C is a column vector of c_p, U is the unit matrix, and the matrices A and Γ elements are for $p\geq 0$

$$a_{p0}=\int_0^\infty \beta_1 g(\zeta)f_0(\zeta)f_p(\zeta)\zeta\,d\zeta \tag{2.10}$$

$$a_{pn}=\int_0^\infty k_{zn}g(\zeta)f_n(\zeta)f_p(\zeta)\zeta\,d\zeta,\quad n\geq 1 \tag{2.11}$$

$$\gamma_p=-a_{p0}-\delta_{p0} \tag{2.12}$$

$$g(\zeta)=-i\frac{\epsilon_2}{\epsilon_1}\frac{\cot(\kappa h)}{\kappa} \tag{2.13}$$

where δ_{p0} is the Kronecker delta.

It is possible to evaluate a_{pn} in rapidly converging series by utilizing the residue calculus. By appropriately choosing a contour path similar as in [5], we obtain

$$a_{00}=-i\sqrt{\frac{\epsilon_2}{\epsilon_1}}\cot\beta_2 h-\frac{\beta_1}{2}\sum_{m=0}^{\infty}\pi M_0^2\alpha_m\frac{\Lambda_{00}(\xi_m)}{h\xi_m^2} \tag{2.14}$$

$$a_{0n}=\frac{\pi k_{zn}}{2h}\sum_{m=0}^{\infty}\alpha_m\phi_n(\xi_m)\Lambda_{10}(\xi_m) \tag{2.15}$$

$$a_{p0}=\frac{\pi\beta_1}{2h}\sum_{m=0}^{\infty}\alpha_m\phi_p(\xi_m)\Lambda_{01}(\xi_m) \tag{2.16}$$

$$a_{pn}=\frac{\epsilon_2 M_n^2\cot\left(\sqrt{\beta_2^2-k_n^2}\,h\right)}{\epsilon_1\pi k_n J_0^2(k_n a)}\Lambda_{11}'(k_n)\delta_{pn}-\frac{\pi k_{zn}}{2h}\sum_{m=0}^{\infty}\alpha_m\psi_{pn}(\xi_m)\Lambda_{11}(\xi_m) \tag{2.17}$$

where $\Lambda_{11}'(k_n)$ denotes $[d\Lambda_{11}(\zeta)/d\zeta]|_{\zeta=k_n}$, and

$$\begin{aligned}\Lambda_{st}(\zeta)=&[J_0(sak_n)J_0(tak_p)J_0(b\zeta)H_0^{(1)}(b\zeta)\\&-J_0(sak_n)J_0(tbk_p)J_0(a\zeta)H_0^{(1)}(b\zeta)\\&-J_0(sbk_n)J_0(tak_p)J_0(a\zeta)H_0^{(1)}(b\zeta)\\&+J_0(sbk_n)J_0(tbk_p)J_0(a\zeta)H_0^{(1)}(a\zeta)]\frac{\epsilon_2}{\epsilon_1}\end{aligned} \tag{2.18}$$

$$s,\,t=1,\,0$$

$$\xi_m=\sqrt{\beta_2^2-\left(\frac{m\pi}{h}\right)^2},\quad m=0,\,1,\,2,\,\cdots \tag{2.19}$$

$$\phi_n(\zeta)=\frac{2M_0M_n}{\pi k_n J_0(k_n a)(k_n^2-\zeta^2)} \tag{2.20}$$

$$\psi_{pn}(\zeta)=\frac{4M_pM_n\zeta^2}{\pi^2k_pk_nJ_0(k_pa)J_0(k_na)(k_p^2-\zeta^2)(k_n^2-\zeta^2)} \tag{2.21}$$

$$\alpha_m=\begin{cases}1, & m=0\\ 2, & m\geq 1.\end{cases} \tag{2.22}$$

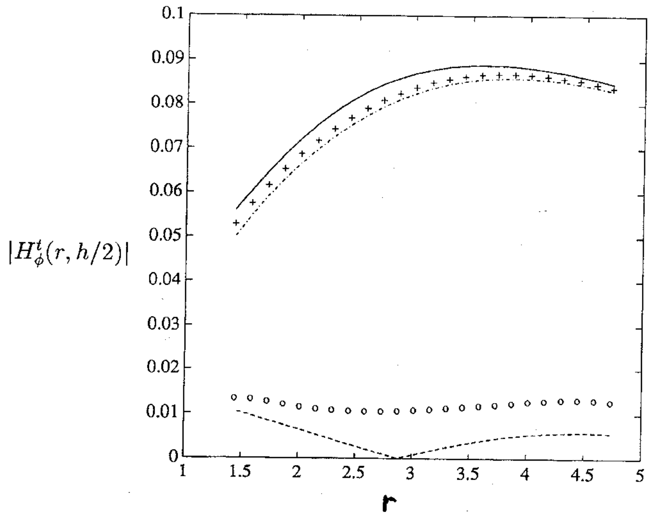

Fig. 2. $H_\phi^t(r,\,z)$ field comparison with [4]. [$a=1.4264$ mm, $b=4.7250$ mm, $\epsilon_1=\epsilon_2=2.08\epsilon_0$, $z=h/2$, $h/b=1$, $f=10$ GHz, ϵ_0: air permittivity, + + + Tomasic [4]; –.–.– first term in (2.23); o o oo second term in (2.23); – – – third term in (2.23); ——— $H_\phi^t(r,\,z)$ (first + second + third terms).

From (2.3) and (2.5), we obtain the transmitted H-field as

$$\begin{aligned}H_\phi^t(r,\,z)=\;&B_1\sum_{m=0}^{\infty}\begin{cases}\dfrac{\alpha_m}{\sqrt{1-\left(\frac{m\pi}{\beta_2 h}\right)^2}}\cos\dfrac{m\pi}{h}z\cdot[J_0(\xi_m b)-J_0(\xi_m a)]H_1^{(1)}(\xi_m r)\\[2ex] \dfrac{\alpha_m}{\sqrt{1-\left(\frac{m\pi}{\beta_2 h}\right)^2}}\cos\dfrac{m\pi}{h}z\cdot[J_1(\xi_m r)H_0^{(1)}(\xi_m b)-H_1^{(1)}(\xi_m r)J_0(\xi_m a)]-\dfrac{2hi}{\pi r}\dfrac{\cos\beta_2(h-z)}{\sin\beta_2 h}\delta_{m0}\\[2ex] \dfrac{\alpha_m}{\sqrt{1-\left(\frac{m\pi}{\beta_2 h}\right)^2}}\cos\dfrac{m\pi}{h}z\cdot J_1(\xi_m r)[H_0^{(1)}(\xi_m b)-H_0^{(1)}(\xi_m a)]\end{cases}\\&-\sum_{n=1}^{\infty}\sum_{m=0}^{\infty}B_2\frac{\cos\frac{m\pi}{h}z}{k_n^2-\xi_m^2}\times\begin{cases}[J_0(\xi_m b)J_0(k_n a)-J_0(\xi_m a)J_0(k_n b)]H_1^{(1)}(\xi_m r)\\ J_1(\xi_m r)J_0(k_n a)H_0^{(1)}(\xi_m b)-H_0^{(1)}(\xi_m r)J_0(\xi_m a)J_0(k_n b)\\ J_1(\xi_m r)[H_0^{(1)}(\xi_m b)J_0(k_n a)-H_0^{(1)}(\xi_m a)J_0(k_n b)]\end{cases}\\&-\sum_{n=1}^{\infty}\frac{\epsilon_2 c_n k_{zn}M_n}{\epsilon_1}\frac{i\cos\kappa_n(h-z)}{\kappa_n\sin\kappa_n h}\times\begin{cases}0, & r\geq b\\ N_0(k_nb)J_1(k_nr)-J_0(k_nb)N_1(k_nr), & a\leq r\leq b\\ 0, & r\leq a\end{cases}\end{aligned} \tag{2.23}$$

where $B_1=-\sqrt{\epsilon_2/\mu_0}\,[\pi V_0]/[2h\ln(b/a)]$, $B_2=[2c_n\epsilon_2k_{zn}\xi_m^2M_n\alpha_m]/[\epsilon_1k_nJ_0(k_na)h]$, $V_0=[\beta_1(1-c_0)]/[\omega\epsilon_1M_0]$, and $\kappa_n=\sqrt{k_2^2-k_n^2}$.

The comparison of the first term in (2.23) with (25) in [4] reveals a difference in the expressions between them for $a\leq r\leq b$. Fig. 2 shows a field distribution $|H_\phi^t(r,\,h/2)|$ for $a<r<b$, confirming a slight difference between the first

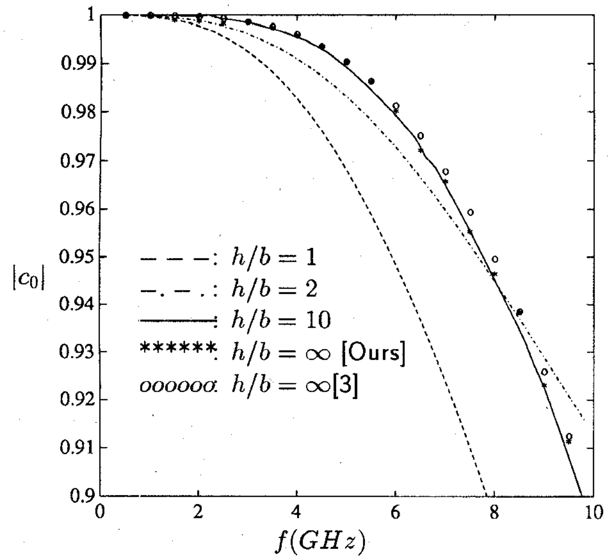

Fig. 3. Reflection coefficient $|c_0|$ versus frequency (a = 1.4264 mm, b = 4.7250 mm, $\epsilon_1 = \epsilon_2 = 2.08\epsilon_0$).

term in (2.23) and (25) in [4]. Fig. 2 further shows that in low-frequency limit ($\lambda \gg a$, b and $|c_0| \gg |c_1|, |c_2|, \cdots$) the second and third terms containing c_n ($n \geq 1$) in (2.23) may be ignored.

When the flanged coaxial line radiates into a half-space ($h \to \infty$), the solution given in (2.9)–(2.12) is still applicable by replacing (2.13) with $g(\zeta) = -\epsilon_2/(\epsilon_1\kappa)$. Performing the branch-cut integration of (2.10) and (2.11), we obtain a_{pn} in numerically efficient, fast converging integral forms for $h \to \infty$

$$a_{00} = -\sqrt{\frac{\epsilon_2}{\epsilon_1}} + \beta_1 \int_0^\infty \frac{M_0^2}{\kappa\zeta} \Lambda_{00}(\zeta) i\, dv \quad (2.24)$$

$$a_{0n} = -k_{zn} \int_0^\infty \frac{\zeta}{\kappa} \phi_n(\zeta)\Lambda_{10}(\zeta) i\, dv \quad (2.25)$$

$$a_{p0} = -\beta_1 \int_0^\infty \frac{\zeta}{\kappa} \phi_p(\zeta)\Lambda_{01}(\zeta) i\, dv \quad (2.26)$$

$$a_{pn} = -\frac{i\epsilon_2 M_n^2}{\epsilon_1 \pi k_n J_0^2(k_n a)} \Lambda'_{11}(k_n)\delta_{pn} + k_{zn} \int_0^\infty \frac{\zeta}{\kappa} \psi_{pn}(\zeta)\Lambda_{11}(\zeta) i\, dv \quad (2.27)$$

TABLE I
CONVERGENCE RATE OF $|c_n|$ VERSUS n WHEN $h/b = 10$. (OTHER PARAMETERS USED ARE THE SAME AS IN FIG. 3)

Freq.[GHz]	0.5	5.0	9.5
n	$\lvert c_n\rvert$	$\lvert c_n\rvert$	$\lvert c_n\rvert$
0	0.999996	0.989252	0.926587
1	0.002953	0.034111	0.067913
2	0.000948	0.009146	0.016410
3	0.000320	0.003624	0.006818

where $\zeta = \beta_2 + iv$. Note that (2.24)–(2.27) are numerically more efficient than (2.10)–(2.11).

Fig. 3 shows the behavior of the reflection coefficient $|c_0|$ versus frequency for different h/b. When $h/b \to \infty$, our results agree with [3]. When $h/b > 10$, $|c_0|$ is almost the same as that for $h/b \to \infty$. Table I shows the rate of convergence for $|c_n|$ when $h/b = 10$. In Fig. 3, we use $n = 0$, 1 to achieve the numerical accuracy. This means that our series solution converges very rapidly thus numerically efficient.

III. CONCLUSION

Reflection of a coaxial line radiating into a parallel plate is solved with the Hankel transform and the mode-matching technique. An analytic series solution is obtained and its numerical computations are performed to illustrate the reflection behavior. The presented series solution is a rigorous, closed-form that is simple and efficient for numerical computation.

REFERENCES

[1] H. Levine and C. H. Papas, "Theory of the circular cylinder diffraction antenna," *J. Appl. Phys.*, vol. 22, no. 1, pp. 29–43, Jan. 1951.
[2] D. C. Chang, "Input admittance and complete near-field distribution of an annular aperture antenna driven by a coaxial line," *IEEE Trans. Antennas Propagat.*, vol. AP-18, no. 5, pp. 610–616, Sept. 1970.
[3] J. R. Mosig, J. E. Besson, M. Gex-Fabry, and F. E. Gardiol, "Reflection of an open-ended coaxial line and application to nondestructive measurement of materials," *IEEE Trans. Instrum. Meas.*, vol. IM-30, no. 1, pp. 46–51, Mar. 1981.
[4] B. Tomasic and A. Hessel, "Electric and magnetic current sources in the parallel plate waveguide," *IEEE Trans. Antennas Propagat.*, vol. AP-45, no. 11, pp. 1307–1310, Nov. 1987.
[5] P. M. Morse and K. U. Ingard, *Theoretical Acoustics*. New York: McGraw-Hill, p. 640.